Atherosclerosis 284 (2019) 187–193

Contents lists available at ScienceDirect

Atherosclerosis

journal homepage: www.elsevier.com/locate/atherosclerosis

Morphometry and hemodynamics of coronary artery aneurysms caused by atherosclerosis

Tingting Fan[a,b], Zhen Zhou[c], Wenxuan Fang[a,b], Wenjing Wang[c], Lei Xu[c,**], Yunlong Huo[a,b,*]

[a] Department of Mechanics and Engineering Science, College of Engineering, Peking University, Beijing, China
[b] PKU-HKUST Shenzhen-Hongkong Institution, Shenzhen, China
[c] Department of Radiology, Beijing Anzhen Hospital, Capital Medical University, Beijing, China

HIGHLIGHTS

- A two-step analysis method is proposed to improve the risk assessment of CAAs due to atherosclerosis.
- Patients with the CAA covering a bifurcation have the higher occurrence of myocardial ischemia.
- Patients with the CAA of L/W ≥ 2 covering a bifurcation show the worst hemodynamic environment.

ARTICLE INFO

Keywords:
Coronary artery aneurysm
CTA (computed tomography angiography)
Hemodynamics

ABSTRACT

Background and aims: Atherosclerosis is the first etiology of coronary artery aneurysm (CAA). It is, however, challenging to inhibit the development of CAA. The aim of the study is to carry out morphometric and hemodynamic analyses in epicardial coronary arteries of patients with CAAs caused by atherosclerosis.
Methods: Various morphometric parameters were obtained from the reconstructed epicardial coronary arterial trees of 61 patients and multiple hemodynamic parameters were determined from the computed flow fields. A two-step analysis method was proposed to enhance the risk assessment of CAAs, i.e., coronary artery bifurcation is the major risk factor for CAA followed by high aneurysm shape index (L/W, where L and W refer to the aneurysm length and maximum diameter, respectively).
Results: Patients with CAA covering a bifurcation have the higher occurrence (71% and 55% for L/W ≥ 2 and L/W < 2, respectively) of myocardial ischemia relevant to abnormal hemodynamic parameters in comparison with those with CAA in one vessel (43% and 40% for L/W ≥ 2 and L/W < 2, respectively). Patients with CAA of L/W ≥ 2 covering a bifurcation show the worst hemodynamic environment.
Conclusions: Morphometric and hemodynamic studies support the two-step analysis method, which provides a clinical rationale for the noninvasive assessment of CAAs.

1. Introduction

Coronary artery aneurysm (CAA) is an abnormal dilatation of coronary artery [6] with an incidence of 1.2–4.9% [7]. The ratio of male to female patients has an approximate value of 3:1 [7]. Coronary atherosclerosis is the first cause of CAA [8,9]. Patients with CAAs often have high blood pressure or have the habit of smoking [6]. Stable angina is the most common feature in patients with CAAs [10], while myocardial infarction (MI) occurs owing to the distal embolization or occlusion of ectatic segment with thrombus [11,12]. Although CAA treatment varies from medical control to stent insertion and surgical ligation, long-term prognosis is still controversial and uncertain.

Morphometric and hemodynamic studies have been carried out to investigate various intracranial aneurysms [13–22]. Multiple parameters were used to assess the rupture of intracranial aneurysms despite much debate. In comparison with substantial hemodynamic studies of intracranial aneurysms, there are relatively few investigations of CAAs. Marsden and colleagues have recently performed image-based modeling of hemodynamics in patient-specific CAAs as a result of Kawasaki disease [23,24]. They proposed several hemodynamic parameters for potential risk assessment of CAAs, e.g., low wall shear stress (WSS) within the aneurysm and high WSS gradient (WSSG) at

* Corresponding author. Department of Mechanics and Engineering Science, College of Engineering, Peking University, Beijing, 100871, China.
** Corresponding author.
E-mail addresses: leixu2001@aliyun.com (L. Xu), yhuo@pku.edu.cn (Y. Huo).

https://doi.org/10.1016/j.atherosclerosis.2019.03.001
Received 3 September 2018; Received in revised form 18 February 2019; Accepted 22 February 2019
Available online 08 March 2019
0021-9150/

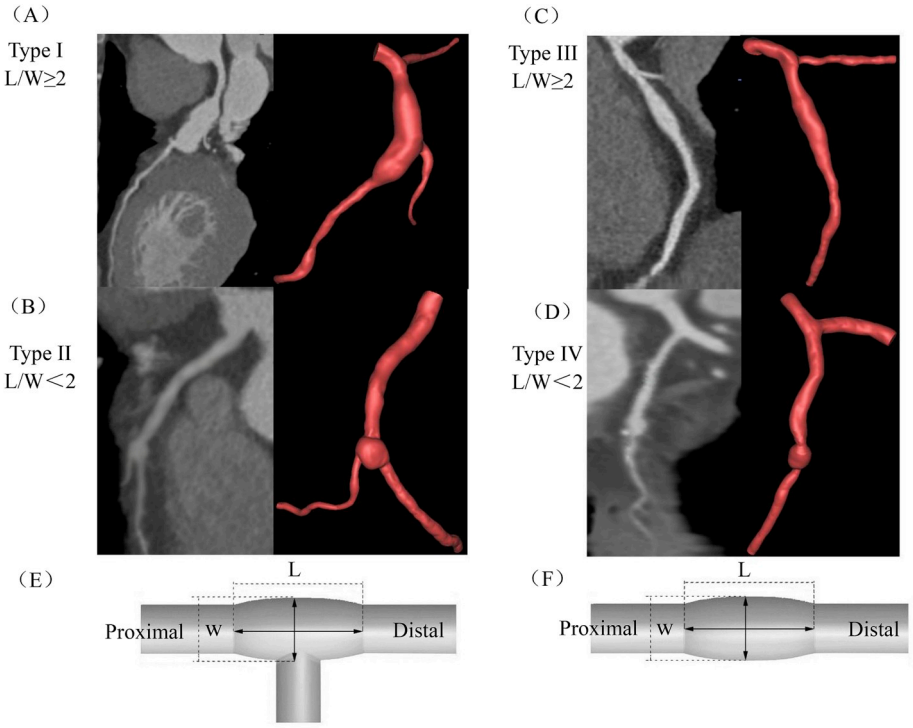

Fig. 1. (A–D) Epicardial coronary arteries with aneurysms of types I-IV reconstructed from CTA images of representative patients. (E) Schematic representative of CAAs of types I and III, corresponding to panels A and B. (F) Schematic representative of CAAs of types II and IV corresponding to panels C and D.

aneurysmal necks for developing thrombotic risk stratification. There is, however, a lack of hemodynamic studies in patient-specific CAAs as a result of coronary atherosclerosis, which requires more investigations.

The objective of the study was to perform morphometric and hemodynamic analyses in epicardial coronary arteries with aneurysms as a result of coronary atherosclerosis. Here, we propose a novel two-step analysis method to enhance the risk assessment of CAA, i.e., myocardial ischemia after thrombus formation. Three-dimensional (3D) geometrical models of epicardial coronary arteries with CAAs were reconstructed from CTA images. We determined multiple morphometric parameters and further classified CAAs into 4 types. A transient 3D finite volume model (FVM) was used to solve the continuity and Navier-Stokes equations to compute the flow fields in epicardial coronary arteries with CAAs, from which hemodynamic parameters (including velocity, velocity curl, time-averaged wall shear stress-TAWSS, oscillatory shear index-OSI, and TAWSS spatial gradient-TAWSSG) were obtained. The significance, implication and limitation of the study were discussed to aid in clinical decision making.

2. Materials and methods

2.1. Study design

The study retrospectively analyzed the hemodynamics in 61 patients with CAAs, who underwent the CTA of coronary arteries at the Beijing Anzhen Hospital, Beijing, China. A total of 80 coronary artery aneurysms were identified. The study was approved by the Institutional Review Board (IRB) for the Beijing Anzhen Hospital, which conforms the declaration of Helsinki.

2.2. Imaging acquisition and electrocardiogram interpretation

Similar to previous studies [5,25,26], prior to imaging acquisition, patients were given the repeated doses of intravenous metoprolol of 5 mg every 5 min until heart rate was ≤70 bpm or a maximum dose of 15 mg was given. Some patients received sublingual nitroglycerin tablet (0.4 mg) 3–5 min before CTA examination.

Coronary CTA (CCTA) was performed through three CT scanners (i.e., 256-row detector CT scanner [Revolution CT, GE Healthcare, Milwaukee, USA], 320–detector row [Aquilion One; Toshiba, Otawara, Japan], or dual-source [Somatom Definition Flash; Siemens, Forchheim, Germany] CT) according to the guidelines of the Society of cardiovascular computed tomography [27]. The CCTA images were acquired when 50–60 ml contrast agent (370 mg iodine/ml, Ultravist, Bayer Schering Pharma, Berlin, Germany) was injected at a rate of 4.5–5 ml/s followed by IV (Intravenous) injection of saline chase of 30–35 ml at a rate of 5 ml/s, similar to a previous study [28].

For all of scanners, prospective electrocardiography gating and bolus tracking were used for image acquisition. Gantry rotation time was 0.28 or 0.35 s per rotation. Tube voltage of 100 or 120 kV with automatically selected tube current were used for image acquisition, and transaxial images were reconstructed with 0.5, 0.6, or 0.625 mm section thickness. For helical images, the position of the reconstruction window within the cardiac cycle was individually selected to minimize artifacts. Motion-free data sets were collected for analysis. All studies were considered diagnostic image quality with optimal contrast enhancement and no substantial motion artifacts.

ST-segment and T-wave abnormalities were used for evaluation of myocardial ischemia according to 'AHA/ACCF/HRS Recommendations for the Standardization and Interpretation of the Electrocardiogram' [29,30].

2.3. 3D reconstruction and geometrical model

All digitized data were imported into the MIMICS Innovation Suite platform (Materialise Company, Belgium) to obtain the 3D geometries, as shown in Fig. 1 [31,32]. Morphometric data of epicardial coronary arteries with CAA were extracted. A centerline was formed by a series of center points in the center on the cross–sectional views of the contour of the 3D vessel while the best fit diameter, D_{fit}, was calculated as twice the average radius between the point on the centerline and the contour forming the contour of the 3D vessel [5,25]. Moreover, morphometric

Table 1
Demographics of the study population.

	Type I	Type II	Type III	Type IV
Patient No. (aneurysm No.)	7 (10)	11 (18)	23 (29)	20 (23)
Age (year)	56 ± 12	51 ± 19	51 ± 18	58 ± 11
Male (%)	100	77	68	55
Myocardial ischemia (%)	71	55	43	40
Hypertension (%)	56	62	57	59
Hyperlipidemia (%)	42	45	40	64
Diabetes mellitus (%)	0	23	0	18
Smoking (%)	100	46	40	45
Systolic blood pressure (mmHg)	122 ± 14	131 ± 11	124 ± 19	125 ± 13
Diastolic blood pressure (mmHg)	77 ± 15	76 ± 2	78 ± 11	77 ± 13
Fasting glucose (mmol/L)	5.3 ± 0.6	5.9 ± 1.0	5.3 ± 0.7	6.8 ± 3.3
Triglycerides (mmol/L)	1.5 ± 0.5	2.0 ± 0.5	1.9 ± 1.7	3.3 ± 4.3
LDL (mmol/L)	2.0 ± 0.7	2.1 ± 0.5	2.1 ± 0.5	2.6 ± 0.6
HDL (mmol/L)	1.0 ± 0.1	1.3 ± 0.4	1.0 ± 0.2	1.1 ± 0.3
Total cholesterol (mmol/L)	3.5 ± 0.8	4.2 ± 0.4	3.8 ± 0.6	4.8 ± 1.3
BMI (kg/m^2)	27.2 ± 2.6	26.2 ± 3.0	25.1 ± 6.2	26.1 ± 2.9

LDL: low density lipoprotein; HDL: high density lipoprotein; BMI: body mass index.

parameters, W (maximum aneurysm diameter), L (aneurysm length), L/W (aneurysm shape index), and φ (sphericity index = $\frac{\pi^{1/3}\cdot(6V)^{2/3}}{A}$, where V is the aneurysm volume and A is the surface area) in Fig. 1E and F, were determined in each aneurysm. The reconstruction and imaging analysis were performed by a student (Tingting Fan) at the College of Engineering, Peking University as well as a Radiologist (Zhen Zhou) at the Beijing Anzhen Hospital. The reproducibility of the measurements showed κ value equals to 0.86.

Based on morphometric data, geometrical models were meshed using the ANSYS ICEM software (ANSYS Inc., Canonsburg, USA) and then smoothed using the Geomagic Studio software (3D Systems, Rock Hill, USA). Similar to previous studies [5,25], a mesh dependency was conducted such that the relative error in two consecutive mesh refinements was < 1% for TAWSS. A total of approximately 500,000 tetrahedral shaped volume elements (element size = 0.25 mm) were necessary to accurately mesh the computational domain.

2.4. Computational model

The Navier-Stokes and continuity equations were solved using a finite volume solver, FLUENT (ANSYS Inc., Canonsburg, USA). Coronary arteries and aneurysms were assumed to be rigid and impermeable. Three cardiac cycles were required to achieve convergence for the transient analysis similar to previous studies [5,25,26,33]. A constant time step was employed, where $\Delta t = 0.01$ s with 84 total time steps per cardiac cycle. The aortic pulsatile pressure wave, as shown in Supplementary Fig.1, was measured in a representative patient and applied to the inlet of epicardial coronary arterial tree. The resistance boundary condition (see details in the Appendix) was assigned to each outlet. Although blood is a suspension of particles, it behaves as a Newtonian fluid in vessels with diameters > 1 mm [34]. Moreover, we have recently shown negligible difference of TAWSS and OSI between Newtonian and non-Newtonian (i.e., Carreau fluid) models [33]. Hence, viscosity (μ) and density (ρ) of the solution were set as 4.5×10^{-3} Pa·s and 1060 kg/m^3, respectively, to mimic blood flows with a hematocrit of about 45% in these arteries. Various hemodynamic parameters were determined from the computed flow fields (see details in Supplementary Materials). We further computed SAR-TAWSS [2], SAR-OSI [3,4], and SAR-TAWSSG [1,5] within CAA region and in coronary arteries except for CAA region (see detailed definitions in the nomenclature).

2.5. Statistical analysis

The CAAs were classified as: 1) type I (L/W ≥ 2 and CAA covering a bifurcation), 2) type II (L/W < 2 and CAA covering a bifurcation), 3) type III (L/W ≥ 2 and CAA in one vessel), and 4) type IV (L/W < 2 and CAA in one vessel). Morphometric and hemodynamic parameters were computed as mean ± standard deviation (SD). ANOVA (SigmaStat 3.5) was used to detect the statistical difference of these parameters, where $p < 0.05$ is indicative of statistical difference.

3. Results

Table 1 lists the demographics of 61 patients with 80 CAAs, which includes 10 CAAs of type I, 18 CAAs of type II, 29 CAAs of type III, and 23 CAAs of type IV. There is a high ratio of male patients. There are significantly higher ratios ($p < 0.05$) of patients of types I and II (CAA covering a bifurcation) with myocardial ischemia than those of types III and IV (CAA in one vessel). There is no statistical difference in hypertension, atherosclerosis, and hyperlipidemia among patients of the four types. Table 2 lists morphometric parameters in patients with CAA. Patients of types I and III show similar morphometric parameters (no statistical difference). Surface area and volume of CAA increase ($p < 0.05$) in a sequence of types IV, II, and I (and III) while aneurysm sphericity decreases.

Fig. 1A–D shows the epicardial coronary arteries with aneurysms of types I-IV, respectively, reconstructed from CTA images of representative patients. Fig. 2A–D shows velocity streamlines (unit: $m\cdot s^{-1}$) within the aneurysm at peak systole as well as the color map of flow velocity (unit: $m\cdot s^{-1}$) and the velocity curl (unit: s^{-1}) on three planes sectioned through CAAs of types I, III, II and IV, respectively. The flow distribution is more complex within CAA as compared with coronary arteries except for CAA region. There are stronger flow vortices within CAAs of types I and II than those within CAAs of types III and IV, which results in low WSS and high OSI at the site of main artery opposite to the flow orifice. This is mainly caused by the fractional flow from the side branch. On the other hand, there are significantly higher values of the velocity curl on the surface of CAAs of types III and IV in comparison with CAAs of types I and II.

Fig. 3 shows TAWSS (unit: dynes/cm^2), OSI, and TAWSSG (unit: dynes/cm^3) in the epicardial coronary arteries of four representative patients with CAAs of types I-IV. CAA region has lower TAWSS and higher OSI than other regions of the coronary artery. Owing to the complex distribution of TAWSS, OSI, and TAWSSG, we use the scalar parameters of SAR-TAWSS, SAR-OSI, and SAR-TAWSSG to enhance quantitative representation of the hemodynamic environment. Table 2 lists these hemodynamic parameters (i.e., SAR-TAWSS, SAR-OSI, and SAR-TAWSSG) in patients with CAAs of types I-IV. Furthermore, Fig. S1 shows a comparison of these parameters between CAAs covering a

Table 2
Morphometric and hemodynamic parameters in patients.

	Type I	Type II	Type III	Type IV
Aneurysm No.	10	18	29	23
Morphometric parameters				
Average value of L/W	2.7 ± 0.3	1.3 ± 0.2	3.2 ± 1.1	1.5 ± 0.3
Surface area of aneurysm (mm^2)	445 ± 195	322 ± 292	482 ± 326	168 ± 86
Volume of aneurysm (mm^3)	816 ± 493	399 ± 366	839 ± 744	236 ± 206
Mean D_{fit} of aneurysm (mm)	6.9 ± 1.2	5.3 ± 2.4	5.9 ± 2.1	4.9 ± 2.0
$\frac{\text{Surface area of aneurysm}}{\text{Surface area of vessel}}$	0.27 ± 0.07	0.17 ± 0.07	0.32 ± 0.17	0.13 ± 0.06
$\frac{\text{Volume of aneurysm}}{\text{Volume of vessel}}$	0.43 ± 0.11	0.25 ± 0.11	0.44 ± 0.23	0.18 ± 0.11
L_{chord} (mm)	69 ± 11	66 ± 19	62 ± 14	59 ± 13
L_{arc} (mm)	84 ± 13	85 ± 31	88 ± 32	86 ± 44
L_{chord}/L_{arc}	0.82 ± 0.05	0.80 ± 0.08	0.74 ± 0.14	0.76 ± 0.20
Aneurysm sphericity (φ)	0.86 ± 0.06	0.93 ± 0.27	0.85 ± 0.09	1.01 ± 0.13
Hemodynamic parameters within the CCA region				
SAR-WSS (%)	45.4 ± 13.9 $p < 0.05$	23.9 ± 5.1	30.7 ± 8.8 $p < 0.05$	11.4 ± 8.2
SAR-OSI (%)	6.7 ± 5.2 $p < 0.05$	0.3 ± 0.2	6.7 ± 5.6 $p < 0.05$	2.2 ± 2.9
SAR-WSSG (%)	7.3 ± 4.9 $p = 0.14$	3.7 ± 3.2	6.8 ± 11.6 $p = 0.39$	4..9 ± 3.7
Hemodynamic parameters in coronary arteries except for the CAA region				
SAR-WSS (%)	14.8 ± 3.1 $p < 0.05$	6.4 ± 8.0	6.2 ± 9.2 $p < 0.05$	1.0 ± 0.4
SAR-OSI (%)	0.1 ± 0.1 $p = 0.47$	0.0 ± 0.0	0.0 ± 0.0 $p = 0.10$	0.0 ± 0.0
SAR-WSSG (%)	46.9 ± 24.9 $p = 0.33$	50.0 ± 27.4	41.3 ± 17.8 $p = 0.29$	35.3 ± 5.9

Mean D_{fit} of aneurysm (mm): Dfit averaged diameter of the aneurysm.
L_{arc}: the accumulative length along the centerline of coronary artery; L_{chord} : the straight length from inlet to outlet of coronary artery.

bifurcation and CAAs in one vessel. SAR-TAWSS and SAR-OSI values are significantly higher in CAAs with L/W ≥ 2 (CAAs of types I and III) than those in CAAs with L/W < 2 (CAAs of types II and IV). SAR-TAWSS values within CAA region increase in a sequence of types IV, II, III, and I. There is no statistical difference of SAR-TAWSSG between patients of the four types despite higher values in the segment distal to the CAA.

4. Discussion

In comparison with invasive coronary angiography and intravascular ultrasound (IVUS), noninvasive CTA method is routinely used to assess CAAs [35]. Here, 3D geometry of the epicardial coronary arterial tree was reconstructed from CTA images. Based on morphometric data extracted from 61 patients with 80 CAAs due to coronary atherosclerosis, we computed various hemodynamic parameters. The key findings are reported as: 1) both aneurysm shape index (L/W) and coronary artery bifurcation significantly affect the hemodynamics within CAA region and 2) patients with CAA of type I have the highest value of SAR-TAWSS within CAA region and the highest occurrence of myocardial ischemia. The two findings can improve thrombotic risk assessment and aid in clinical decision making.

The ratio of male to female patients with CAAs owing to coronary atherosclerosis agrees with previous studies [7–9], which could be associated with smoking (male: 72.5% *vs.* female: 11.1%). There is also a high ratio of patients with myocardial ischemia similar to a previous study [36]. Multiple morphometric parameters have been proposed for CAA assessment [9,12], for example, giant CAAs (the maximal diameter of CAAs > 8 mm) were suggested to take the clinical treatment [37]. There is, however, much debate for the long prognosis and outcome of CAAs [6]. Hence, hemodynamic analyses were suggested having potentials to provide insights into the effects of aneurysms and to help risk stratify patients for appropriate medical and surgical interventions [23,24]. Low WSS, high OSI, and high WSSG, resulting from stagnation flow, reversal flow, and flow vortex [22,31,38,39], were assumed to be associated with the increased risk by thrombosis [23,24]. The localized distribution of WSS, OSI and WSSG over a cardiac cycle cannot be quantified easily given the complexity of aneurysmal geometry and the pulsatility of blood flow. Hence, we defined the novel parameters, i.e., SAR-TAWSS, SAR-OSI, and SAR-TAWSSG in CAA similar to previous studies [5,22]. These studies only showed a logic starting point toward developing such a hemodynamic framework, which still needs more investigations.

Various morphometric parameters have been proposed to predict the intracranial aneurysm rupture [22], e.g., dome height/dome diameter, dome height/semi-axis height, dome height/neck width, dome diameter/neck width, dome height/upstream diameter, aneurysmal angle, and so on. In comparison with intracranial elastic arteries, coronary muscular arteries are more difficult to have giant CAAs [9], which is consistent with the present CTA observation (6 giant CAAs in 80 CAAs due to coronary atherosclerosis). Aneurysm shape index and coronary artery bifurcation were found to be more accurate to characterize CAAs in comparison with other morphometric parameters. Hence, we classified the CAAs into four types in the study. Patients of the four types have no statistical difference of atherosclerosis, hypertension, and hyperlipidemia. A comparison between types IV and II (L/W < 2) and types I and III (L/W ≥ 2) shows higher surface area and volume of CAA and lower aneurysm sphericity within CAA region of types I and III, which corresponds to higher values of SAR-WSS and SAR-OSI. There are flow vortices of large size within CAA region of types I and III, as shown in Fig. 2, which result in low TAWSS and high OSI and high values of SAR-WSS and SAR-OSI in Fig. 3. This shows the significant effect of aneurysm shape index on the hemodynamics within CAA region, i.e., an increase of L/W deteriorates the hemodynamic environment. However, the increase of L/W does not predict the outcome of CAA completely given the higher occurrence of myocardial ischemia relevant to CAAs of type II as compared with those of type III.

On the other hand, patients with CAAs of types I and II (CAA covering a bifurcation) have the higher occurrence of myocardial ischemia than those with CAAs of types III and IV (CAA in one vessel),

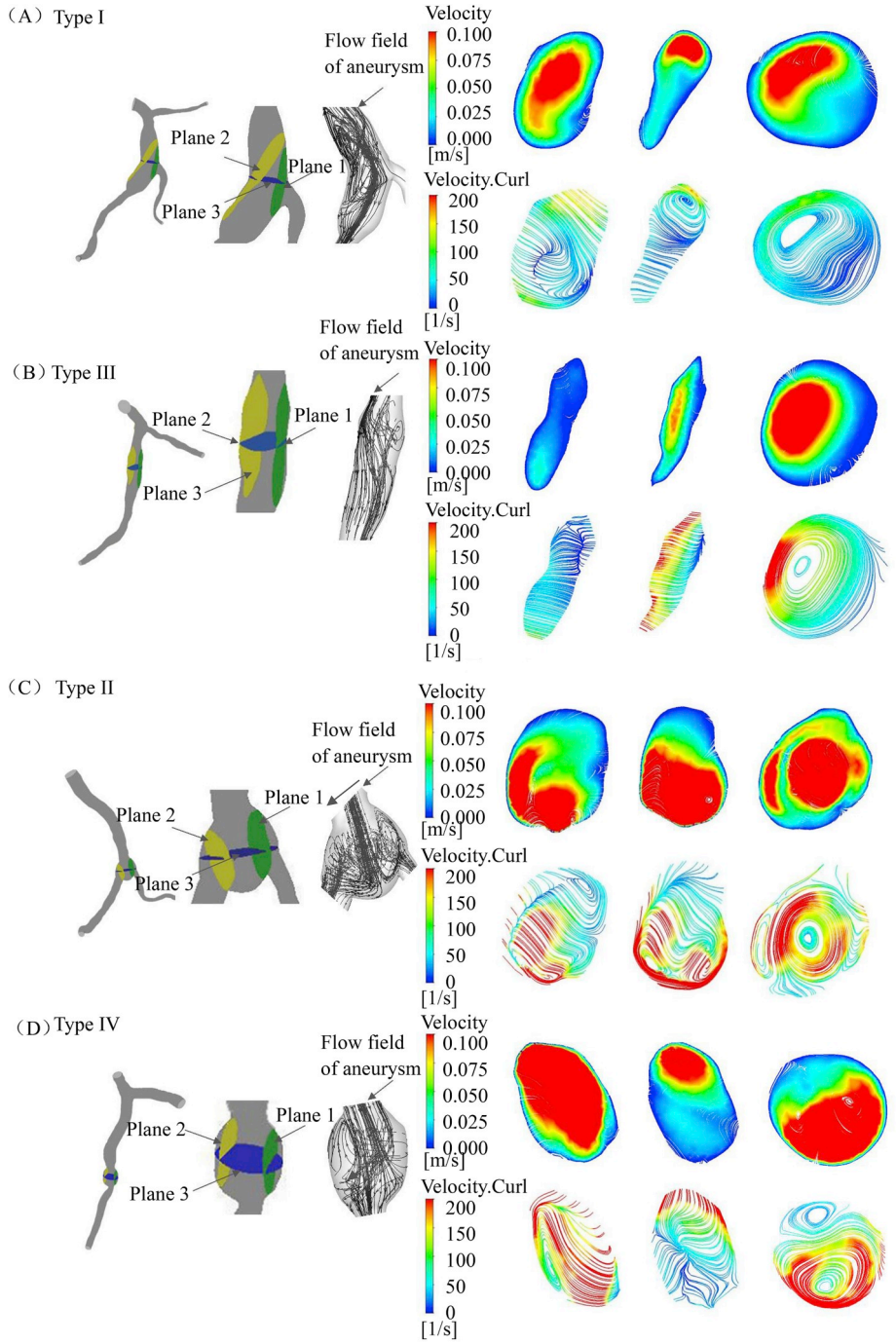

Fig. 2. (A–D) Velocity streamlines (unit: $m \cdot s^{-1}$) within the aneurysm, and color map of flow velocity (unit: $m \cdot s^{-1}$) and velocity curl (unit: s^{-1}) on three planes sectioned through CAAs of type I (A), type III (B), type II (C) and type IV (D). These parameters were plotted at peak systole. (For interpretation of the references to color in this figure legend, the reader is referred to the Web version of this article.)

respectively. Hence, it is required to consider the effect of coronary artery bifurcation on the outcome of CAA given the complex distribution of flow patterns at a bifurcation [39,40]. A two-step analysis method is proposed, i.e., patients with CAAs covering a bifurcation (group 1) predispose to the incidence of myocardial ischemia caused by thrombus formation and distal embolization in comparison with those with CAAs in one vessel (group 2) and further patients with CAAs of high aneurysm shape index predispose to the incidence of myocardial ischemia in each group. CAAs of types I and II have significantly higher values of SAR-TAWSS and SAR-OSI with respect to CAAs of types III and IV. It is known that hypoxia results in inter-endothelial gaps and endothelial cell apoptosis, which increases endothelial permeability to macromolecules, causes high concentration polarization of atherogenic lipids (e.g., low-density lipoprotein-LDL), and promotes inflammation, ATP depletion, and angiogenesis [41–45]. In contrast, the strong velocity curl on the surface of CAAs of types III and IV can enhance oxygen flux to the arterial wall [46], which can delay the thrombus formation in comparison with CAAs of types I and II. Moreover, patients with CAA of type I (CAA covering a bifurcation and $L/W \geq 2$) showed the worst environment of hemodynamics and the highest ratio of myocardial ischemia. These hemodynamic changes support the two-step analysis method.

High TAWSSG can induce strong flow vortices near the arterial wall [1] and hence increase the LDL permeability [38–40], which

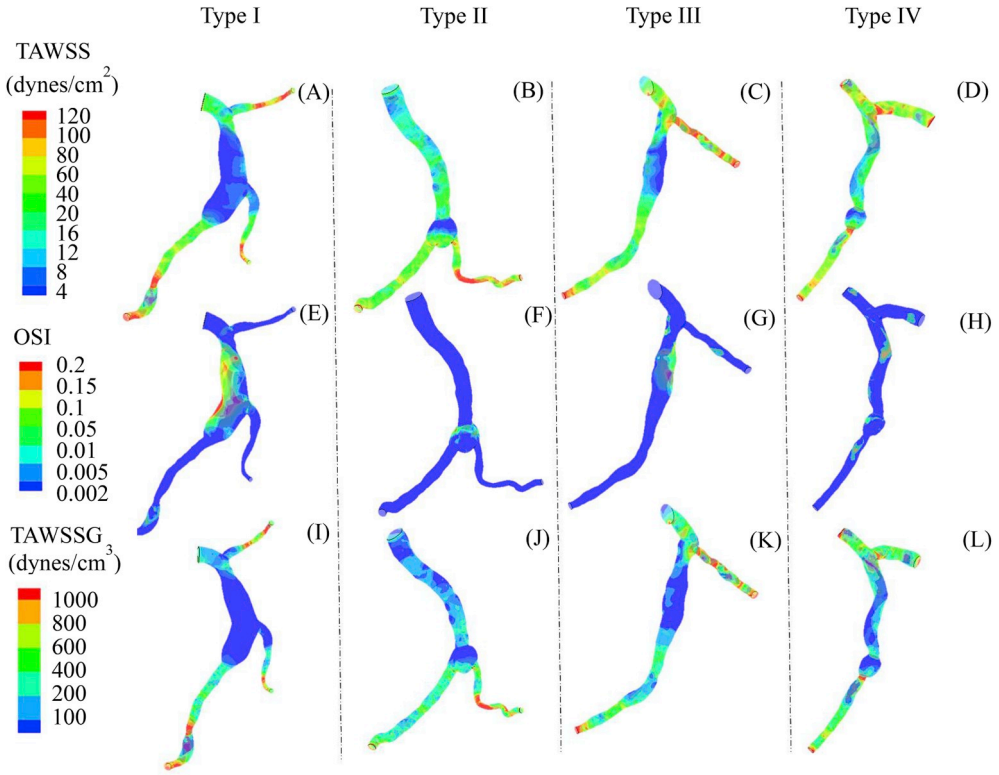

Fig. 3. (A–D) TAWSS (unit: dynes/cm^2), (E–H) OSI, and (I–L) TAWSSG (unit: dynes/cm^3) in epicardial coronary arteries with aneurysms of types I-IV corresponding to Fig. 1A–D.

deteriorates the hemodynamic environment and contributes to the occurrence of myocardial ischemia. Although high TAWSSG occurs in vessel segments distal to the CAA, there is no statistical difference of SAR-TAWSSG between the four groups. Hence, high TAWSSG in distal segments has a relatively small effect on the two-step analysis method.

4.1. Limitations

Since 61 patients with 80 CAAs were a relatively small sample size, a large cohort of patients should be selected to support the proposed two-step analysis method. In comparison with a high risk of rupture for intracranial aneurysms, CAAs predispose to thrombus formation resulting in myocardial ischemia. CAAs show similar flow patterns and hemodynamic parameters to intracranial aneurysms. A future study is required to show molecular and cellular mechanisms associated with abnormal hemodynamic parameters to explain the different risks between CAAs and intracranial aneurysms. Furthermore, passive and active mechanical properties of the vessel wall are of importance to investigate the incidence and progression of CAAs [9,47–49] as well as myocardial ischemia owing to the aneurysm [22]. The effects of triaxial mechanical properties of CAAs on myocardial ischemia should be considered in the following studies when experimental measurements are available.

4.2. Conclusions

Morphometric and hemodynamic analyses were demonstrated in epicardial coronary arteries of 61 patients with 80 CAAs of types I-IV owing to coronary atherosclerosis. We proposed a two-step analysis method to enhance the risk assessment of the CAA, i.e., coronary artery bifurcation is the major risk factor for CAA followed by high aneurysm shape index. Patients with CAAs covering a bifurcation have the higher occurrence of myocardial ischemia and higher values of SAR-TAWSS and SAR-OSI as compared with CAAs in one vessel. Moreover, patients with CAA of L/W ≥ 2 covering a bifurcation showed the highest value of SAR-TAWSS, SAR-OSI, and SAR-TAWSSG and the highest occurrence of myocardial ischemia. This study provided a clinical rationale for the noninvasive assessment of CAAs and warrants future prospective clinical trials.

Conflicts of interest

The authors declared they do not have anything to disclose regarding conflict of interest with respect to this manuscript.

Author contributions

Y. H. wrote the main manuscript text; L. X. performed the clinical trials; T. F. analyzed the CTA images; T. F. and Z. Z. prepared Figs. 1–5; T. F. and W. W. prepared Tables 1–3; and Y. H. and L. X. designed the experiment and revised the main manuscript text. All authors reviewed the manuscript.

Financial support

This research is supported in part by the Natural Science Foundation of China Grant 11672006 (Y. Huo) and Shenzhen Science and Technology R&D Grant JCYJ20160427170536358 (Y. Huo).

Acknowledgements

We thank all participants in the study.

Appendix A. Supplementary data

Supplementary data to this article can be found online at https://doi.org/10.1016/j.atherosclerosis.2019.03.001.

References

[1] C. Kleinstreuer, S. Hyun, J.R. Buchanan, et al., Hemodynamic parameters and early intimal thickening in branching blood vessels, Crit. Rev. Biomed. Eng. 29 (2001) 1–64.
[2] A.M. Malek, S.L. Alper, S. Izumo, Hemodynamic shear stress and its role in atherosclerosis, J. Am. Med. Assoc. 282 (1999) 2035–2042.
[3] Y. Huo, T. Luo, J.M. Guccione, et al., Mild anastomotic stenosis in patient-specific CABG model may enhance graft patency: a new hypothesis, PLoS One 8 (2013) e73769.
[4] H. Nordgaard, A. Swillens, D. Nordhaug, et al., Impact of competitive flow on wall shear stress in coronary surgery: computational fluid dynamics of a LIMA-LAD model, Cardiovasc. Res. 88 (2010) 512–519.
[5] T. Fan, Y. Lu, Y. Gao, et al., Hemodynamics of left internal mammary artery bypass graft: effect of anastomotic geometry, coronary artery stenosis, and postoperative time, J. Biomech. 49 (2016) 645–652.
[6] P.S. Swaye, L.D. Fisher, P. Litwin, et al., Aneurysmal coronary artery disease, Circulation 67 (1983) 134–138.
[7] G.G. Hartnell, B.M. Parnell, R.B. Pridie, Coronary artery ectasia. Its prevalence and clinical significance in 4993 patients, Br. Heart J. 54 (1985) 392–395.
[8] W.C. Roberts, Natural history, clinical consequences, and morphologic features of coronary arterial aneurysms in adults, Am. J. Cardiol. 108 (2011) 814–821.
[9] P.S. Pahlavan, F. Niroomand, Coronary artery aneurysm: a review, Clin. Cardiol. 29 (2006) 439–443.
[10] A.S. Aboeata, S.P. Sontineni, V.M. Alla, et al., Coronary artery ectasia: current concepts and interventions, Front Biosci (Elite Ed) 4 (2012) 300–310.
[11] O. Akyurek, B. Berkalp, T. Sayin, et al., Altered coronary flow properties in diffuse coronary artery ectasia, Am. Heart J. 145 (2003) 66–72.
[12] S. Devabhaktuni, A. Mercedes, J. Diep, et al., Coronary artery ectasia-A review of current literature, Curr. Cardiol. Rev. 12 (2016) 318–323.
[13] S. Dhar, M. Tremmel, J. Mocco, et al., Morphology parameters for intracranial aneurysm rupture risk assessment, Neurosurgery 63 (2008) 185–197.
[14] I. Nikolic, G. Tasic, V. Bogosavljevic, et al., Predictable morphometric parameters for rupture of intracranial aneurysms - a series of 142 operated aneurysms, Turkish Neurosurgery 22 (2012) 420–426.
[15] M.L. Raghavan, B.S. Ma, R.E. Harbaugh, Quantified aneurysm shape and rupture risk, J. Neurosurg. 102 (2005) 355–362.
[16] H. Ujiie, H. Tachibana, O. Hiramatsu, et al., Effects of size and shape (aspect ratio) on the hemodynamics of saccular aneurysms: a possible index for surgical treatment of intracranial aneurysms, Neurosurgery 45 (1999) 119–129.
[17] H. Yu, H. Li, J. Liu, et al., An approach to quantitative assessment of hemodynamic differences between unruptured and ruptured ophthalmic artery aneurysms, Comput. Methods Biomech. Biomed. Eng. 19 (2016) 1456–1461.
[18] L. Parlea, R. Fahrig, D.W. Holdsworth, et al., An analysis of the geometry of saccular intracranial aneurysms, Am. J. Neuroradiol. 20 (1999) 1079–1089.
[19] A.L. Ho, N. Lin, K.U. Frerichs, et al., Intrinsic, transitional, and extrinsic morphological factors associated with rupture of intracranial aneurysms, Neurosurgery 77 (2015) 433–441 ; discussion 441-432.
[20] A. Chien, S. Tateshima, J. Sayre, et al., Patient-specific hemodynamic analysis of small internal carotid artery-ophthalmic artery aneurysms, Surg. Neurol. 72 (2009) 444–450.
[21] V.M. Pereira, O. Brina, P. Bijlenga, et al., Wall shear stress distribution of small aneurysms prone to rupture a case-control study, Stroke 45 (2014) 261–264.
[22] X. Huang, D. Liu, X. Yin, et al., Morphometry and hemodynamics of posterior communicating artery aneurysms: ruptured versus unruptured, J. Biomech. 76 (2018) 35–44.
[23] D. Sengupta, A.M. Kahn, J.C. Burns, et al., Image-based modeling of hemodynamics in coronary artery aneurysms caused by Kawasaki disease, Biomechanics Model. Mechanobiol. 11 (2012) 915–932.
[24] D. Sengupta, A.M. Kahn, E. Kung, et al., Thrombotic risk stratification using computational modeling in patients with coronary artery aneurysms following Kawasaki disease, Biomechanics Model. Mechanobiol. 13 (2014) 1261–1276.
[25] T. Fan, Y. Feng, F. Feng, et al., A comparison of postoperative morphometric and hemodynamic changes between saphenous vein and left internal mammary artery grafts, Phys. Rep. 5 (2017).
[26] X. Chen, Y. Gao, B. Lu, et al., Hemodynamics in coronary arterial tree of serial stenoses, PLoS One 11 (2016) e0163715.
[27] W.G. Weigold, S. Abbara, S. Achenbach, et al., Standardized medical terminology for cardiac computed tomography: a report of the Society of Cardiovascular Computed Tomography, J. Cardiovasc. Comput. Tomogr. 5 (2011) 136–144.
[28] Y. Huo, T. Wischgoll, J.S. Choy, et al., CT-based diagnosis of diffuse coronary artery disease on the basis of scaling power laws, Radiology 268 (2013) 694–701.
[29] P.M. Rautaharju, B. Surawicz, L.S. Gettes, et al., AHA/ACCF/HRS recommendations for the standardization and interpretation of the electrocardiogram: part IV: the ST segment, T and U waves, and the QT interval: a scientific statement from the American heart association electrocardiography and arrhythmias committee, council on clinical cardiology; the American College of cardiology foundation; and the heart rhythm society: endorsed by the international society for computerized electrocardiology, Circulation 119 (2009) e241–250.
[30] G.S. Wagner, P. Macfarlane, H. Wellens, et al., AHA/ACCF/HRS recommendations for the standardization and interpretation of the electrocardiogram: part VI: acute ischemia/infarction: a scientific statement from the American heart association electrocardiography and arrhythmias committee, council on clinical cardiology; the American College of cardiology foundation; and the heart rhythm society: endorsed by the international society for computerized electrocardiology, Circulation 119 (2009) e262–270.
[31] X. Yin, X. Huang, Q. Li, et al., Hepatic hemangiomas alter morphometry and impair hemodynamics of the abdominal aorta and primary branches from computer simulations, Front. Physiol. 9 (2018) 334.
[32] X. Huang, X. Yin, Y. Xu, et al., Morphometric and hemodynamic analysis of atherosclerotic progression in human carotid artery bifurcations, Am. J. Physiol. Heart Circ. Physiol. 310 (2016) H639–H647.
[33] X. Yin, X. Huang, Y. Feng, et al., Interplay of proximal flow confluence and distal flow divergence in patient-specific vertebrobasilar system, PLoS One 11 (2016) e0159836.
[34] W.W. Nichols, D.A. McDonald, McDonald's Blood Flow in Arteries: Theoretic, Experimental, and Clinical Principles, Hodder Arnold, London, 2011 xiv,755 pp..
[35] M. Diaz-Zamudio, U. Bacilio-Perez, M.C. Herrera-Zarza, et al., Coronary Artery Aneurysms and Ectasia: Role of Coronary CT Angiography, Radiographics, vol. 29, a review publication of the Radiological Society of North America, Inc, 2009, pp. 1939–1954.
[36] A. Altinbas, C. Nazli, O. Kinay, et al., Predictors of exercise induced myocardial ischemia in patients with isolated coronary artery ectasia, Int. J. Cardiovasc. Imaging 20 (2004) 3–17.
[37] T. Ohkubo, R. Fukazawa, E. Ikegami, et al., Reduced shear stress and disturbed flow may lead to coronary aneurysm and thrombus formations, Pediatr. Int. 49 (2007) 1–7.
[38] Y. Huo, J.S. Choy, M. Svendsen, et al., Effects of vessel compliance on flow pattern in porcine epicardial right coronary arterial tree, J. Biomech. 42 (2009) 594–602.
[39] Y. Huo, T. Wischgoll, G.S. Kassab, Flow patterns in three-dimensional porcine epicardial coronary arterial tree, Am. J. Physiol. Heart Circ. Physiol. 293 (2007) H2959–H2970.
[40] Y. Huo, G. Finet, T. Lefevre, et al., Which diameter and angle rule provides optimal flow patterns in a coronary bifurcation? J. Biomech. 45 (2012) 1273–1279.
[41] S. Ogawa, H. Gerlach, C. Esposito, et al., Hypoxia modulates the barrier and coagulant function of cultured bovine endothelium. Increased monolayer permeability and induction of procoagulant properties, J. Clin. Investig. 85 (1990) 1090–1098.
[42] H. Matsushita, R. Morishita, T. Nata, et al., Hypoxia-induced endothelial apoptosis through nuclear factor-kappaB (NF-kappaB)-mediated bcl-2 suppression: in vivo evidence of the importance of NF-kappaB in endothelial cell regulation, Circ. Res. 86 (2000) 974–981.
[43] X. Deng, Y. Marois, T. How, et al., Luminal surface concentration of lipoprotein (LDL) and its effect on the wall uptake of cholesterol by canine carotid arteries, J. Vasc. Surg. 21 (1995) 135–145.
[44] X. Liu, F. Pu, Y. Fan, et al., A numerical study on the flow of blood and the transport of LDL in the human aorta: the physiological significance of the helical flow in the aortic arch, Am. J. Physiol. Heart Circ. Physiol. 297 (2009) H163–H170.
[45] L.M. Hulten, M. Levin, The role of hypoxia in atherosclerosis, Curr. Opin. Lipidol. 20 (2009) 409–414.
[46] X. Liu, Y.B. Fan, X.Y. Deng, Effect of spiral flow on the transport of oxygen in the aorta: a numerical study, Ann. Biomed. Eng. 38 (2010) 917–926.
[47] Y. Lu, H. Wu, J. Li, et al., Passive and active triaxial wall mechanics in a two-layer model of porcine coronary artery, Sci. Rep. 7 (2017) 13911.
[48] Y. Huo, X. Zhao, Y. Cheng, et al., Two-layer model of coronary artery vasoactivity, J. Appl. Physiol. 114 (2013) (1985) 1451–1459.
[49] Y. Huo, Y. Cheng, X. Zhao, et al., Biaxial vasoactivity of porcine coronary artery, Am. J. Physiol. Heart Circ. Physiol. 302 (2012) H2058–H2063.

Further reading

[50] J.S. Choy, G.S. Kassab, Scaling of myocardial mass to flow and morphometry of coronary arteries, J. Appl. Physiol. 104 (2008) (1985) 1281–1286.
[51] Y. Huo, G.S. Kassab, Intraspecific scaling laws of vascular trees, J. R. Soc. Interface 9 (2012) 190–200.
[52] W.P. Dole, K.L. Richards, C.J. Hartley, et al., Diastolic coronary artery pressure-flow velocity relationships in conscious man, Cardiovasc. Res. 18 (1984) 548–554.